Metals and Materials International (2020) 26:1757–1765
https://doi.org/10.1007/s12540-019-00500-2

Effect of Rolling and Coiling Temperatures on Microstructure and Mechanical Properties of Medium-Carbon Pipeline Steel

Hyung Lae Kim[1] · Sung Hwan Bang[2] · Jong Min Choi[3] · Nae Hyung Tak[4] · Sang Won Lee[5] · Sung Hyuk Park[5]

Received: 12 August 2019 / Accepted: 6 October 2019 / Published online: 1 November 2019

Abstract
Oil country tubular goods (OCTG) steels with a low yield ratio (yield strength/tensile strength) and excellent impact toughness have recently been demanded to ensure mining performance and safety. From this viewpoint, the optimization of the manufacturing conditions is important because they influence the microstructure and mechanical properties of the steels; in particular, in the case of OCTG steels with carbon contents greater than 0.2 wt%, the finishing mill temperature (FMT) and coiling temperature (CT) strongly affect the microstructure of the final products, which are generally composed of ferrite and pearlite phases. In this study, 0.39C-0.23Si-1.56Mn-0.11Cr steel plates were fabricated under various FMT and CT conditions and their yield strength, tensile strength, and impact energy were investigated. In addition, pipes with diameters of 244 and 508 mm were manufactured via an electric resistance welding method using two of these strips fabricated under two different optimized conditions [(1) FMT = 880 °C and CT = 630 °C and (2) FMT = 800 °C and CT = 690 °C] to analyze the change in mechanical properties induced by the work-hardening effect during the piping process. The results revealed that the FMT and CT are closely related to the volume fraction of the ferrite phase, the grain size and lamellar spacing of the pearlite phase, and the tensile and impact properties of the steel strips; the variations in the microstructure and mechanical properties with the FMT and CT were also discussed in detail.

Keywords OCTG · Medium-carbon steel · Coiling temperature · Finishing mill temperature · Microstructure

1 Introduction

Demand for high-performance steels for oil country tubular goods (OCTG) has recently been increasing in response to increased exploration activities of unconventional reserves; as of 2019, the global OCTG market is estimated to be worth $59 billion because of the demand for vertical and horizontal directional drilling equipment required for the surface and intermediate casing of shale gas [1]. Such OCTG products are generally welded pipes fabricated through the leveling and pipe-forming of hot-rolled steel strips to reduce the manufacturing cost [2, 3]. Moreover, these steel pipelines must have high workability to ensure mining performance and safety because displacement control and plastic deformation occur under many real pipeline conditions in the case of complicated and curved unconventional reserves [4, 5].

To ensure high plasticity, steels used for OCTG have carbon contents greater than 0.2 wt% and consist of a ferrite–pearlite dual phase to provide a low yield ratio (YR) by accommodating the initial deformation in the soft ferrite phase [6]. Their work-hardening behavior also influences their ability to satisfy the required specification grade. Therefore, the microstructure of such steels must be composed of a suitable ferrite–pearlite phase ratio and precipitate formation should be avoided because they can lead to dislocation pile-ups; specifically, for OCTG steels used for pipelines, microstructure control is

Hyung Lae Kim and Sung Hwan Bang have contributed equally to this work.

✉ Sung Hyuk Park
sh.park@knu.ac.kr

[1] Maritime Reactor Fuel Development Team, Korea Atomic Energy Research Institute (KAERI), Daejeon 34057, Republic of Korea

[2] Department of Material Science and Engineering, Seoul National University, Seoul 08826, Republic of Korea

[3] Plate Development Department, Hyundai-Steel, Dangjin 31719, Republic of Korea

[4] Division of Industrial Metrology, Korea Research Institute of Standards and Science, Daejeon 34113, Republic of Korea

[5] School of Materials Science and Engineering, Kyungpook National University, Daegu 41566, Republic of Korea

essential to producing dual-phase steels with a low YR, suitable work-hardening behavior, and high toughness for safety and reliability, as well as high resistance to crack initiation and propagation [7–11].

In the oil and gas pipeline industry, strength criteria have been historically used for pipeline design. However, new developments related to dual-phase steels with high ductility, which are designed by considering various mechanical and metallurgical variables such as thermomechanical processing conditions, crystallographic orientation, and characteristics of grain boundaries and phase interfaces, are required to achieve adequate safety and withstand extreme environmental events such as earthquakes, landslides, and other displacements. Thus, many researchers have proposed the strain-based concept, where both the strain and capacity are considered, as the key to an alternative design methodology based on microstructure control [12, 13]. In particular, various studies on the addition of alloying elements and the optimization of manufacturing conditions such as thermomechanically controlled processes have been conducted to manufacture pipeline steels with carbon contents less than 0.1 wt% and a low YR [14–20]. By contrast, fewer investigations have been reported on the properties of OCTG steels with higher carbon contents (greater than 0.2 wt%) and high work-hardening behavior and consisting of simple phases of ferrite and pearlite.

In reality, the microstructure of hot-rolled steel strips is substantially affected by the rolling and coiling processes and the properties it induces are related to the mechanical properties of the final pipes. Therefore, the present study was focused on the relationship between the rolling and coiling conditions—i.e., the finishing mill temperature (FMT) and coiling temperature (CT)—and the mechanical properties of OCTG steel strips. In addition, the change in the mechanical properties after piping was confirmed for the steel strips manufactured under two different selected conditions; these conditions based on the strain-based design concept resulted in excellent properties, i.e., a low YR and an impact toughness sufficiently high for the material to be used in a harsh environment. The two selected conditions resulted in distinctly different microstructures and may be applicable to commercial production.

2 Experimental Procedure

A 0.39C–0.23Si–1.56Mn–0.11Cr (wt%) steel was used in this experiment; its detailed composition is provided in Table 1. Ingots of this steel were hot rolled under various FMT (760–880 °C) and CT (630–690 °C) conditions to fabricate 10 mm-thick plates using a pilot mill. The manufacturing temperatures may affect the microstructural characteristics [such as the area fraction and grain size of the ferrite and pearlite phases and the interlamellar spacing of pearlite (s_c)] of the hot-rolled plates, which in turn may affect the mechanical properties of the final pipes. Among the investigated temperature conditions, two FMT/CT combinations, which resulted in high impact properties and a low YR of the products, were selected for the industrial fabrication of 10 mm-thick strips. The hot-rolled strips fabricated under two selected FMT/CT conditions were used to manufacture welded pipes with two different diameters (244 and 508 mm) via an electric-resistance welding method. The tensile and impact properties of the strips and pipes were subsequently measured. The tensile tests were performed on specimens with a gauge length of 40 mm at a strain rate of 10^{-2} s^{-1} and at room temperature; the loading axis corresponds to the rolling direction of the strips and to the length of the pipes. The impact tests were carried out in accordance with the Charpy V-notch method (ASTM Standard E23); the notch direction corresponded to the transverse direction. The microstructure of each specimen was observed with an optical microscope after the specimen was polished and etched in nital solution. To confirm the phase transformation temperature of ferrite and pearlite in the 0.4C–0.2Si–1.6Mn–0.1Cr steel, dilatometric tests were performed over a wide range of cooling rates from 1 to 30 °C s^{-1}. The s_c value was predicted from the relationship among the interface energy, temperature, and enthalpy of the Fe–C system. The Avrami equation was used to estimate the amounts of pearlite phase on the basis of the phase transformation behavior. The values required for calculating the Avrami equation were obtained using the Thermo-Calc software with the TCFE2000 database. These predicted values were compared with the experimental results.

3 Results and Discussion

Table 2 shows the results of the tensile and impact tests on the plates fabricated under different FMT and CT conditions. The associated variations in yield strength, tensile strength, YR, and impact properties are mapped in Fig. 1. The yield and tensile strengths tended to increase with decreasing CT; in addition, only the former was highly influenced by the FMT and reached the lowest value when both the FMT and the CT were high. As a result, the smallest YR was observed under high FMT and CT (Fig. 1c). The impact energy distribution

Table 1 Chemical composition of the medium-carbon steels used in the present study

Alloying element	C	Mn	Si	P	S	Cr	Al	N
Content (wt%)	0.39	1.56	0.23	0.011	0.001	0.11	0.05	0.0046

Table 2 Tensile and impact properties of the steel plates fabricated under different finishing mill and coiling temperatures (FMT and CT, respectively: FMT*x*-CT*y*, where *x* and *y* indicate the temperatures in °C)

Condition	Tensile properties				CVN (J)	Fabrication of strip and pipe
	YS (MPa)	TS (MPa)	EL (%)	YR		
FMT840-CT630	513	762	27.3	0.67	20.9	–
FMT880-CT630	511	768	28.4	0.67	15.5	O
FMT800-CT630	544	769	27.6	0.71	25.6	–
FMT840-CT670	448	704	29.0	0.64	16.1	–
FMT800-CT670	455	701	26.8	0.65	20.1	–
FMT760-CT670	501	703	27.5	0.71	33.3	–
FMT760-CT630	506	721	28.0	0.70	29.5	–
FMT840-CT690	420	696	26.9	0.60	13.1	–
FMT800-CT690	458	705	27.1	0.65	20.4	O
FMT760-CT690	511	699	27.5	0.73	27.7	–

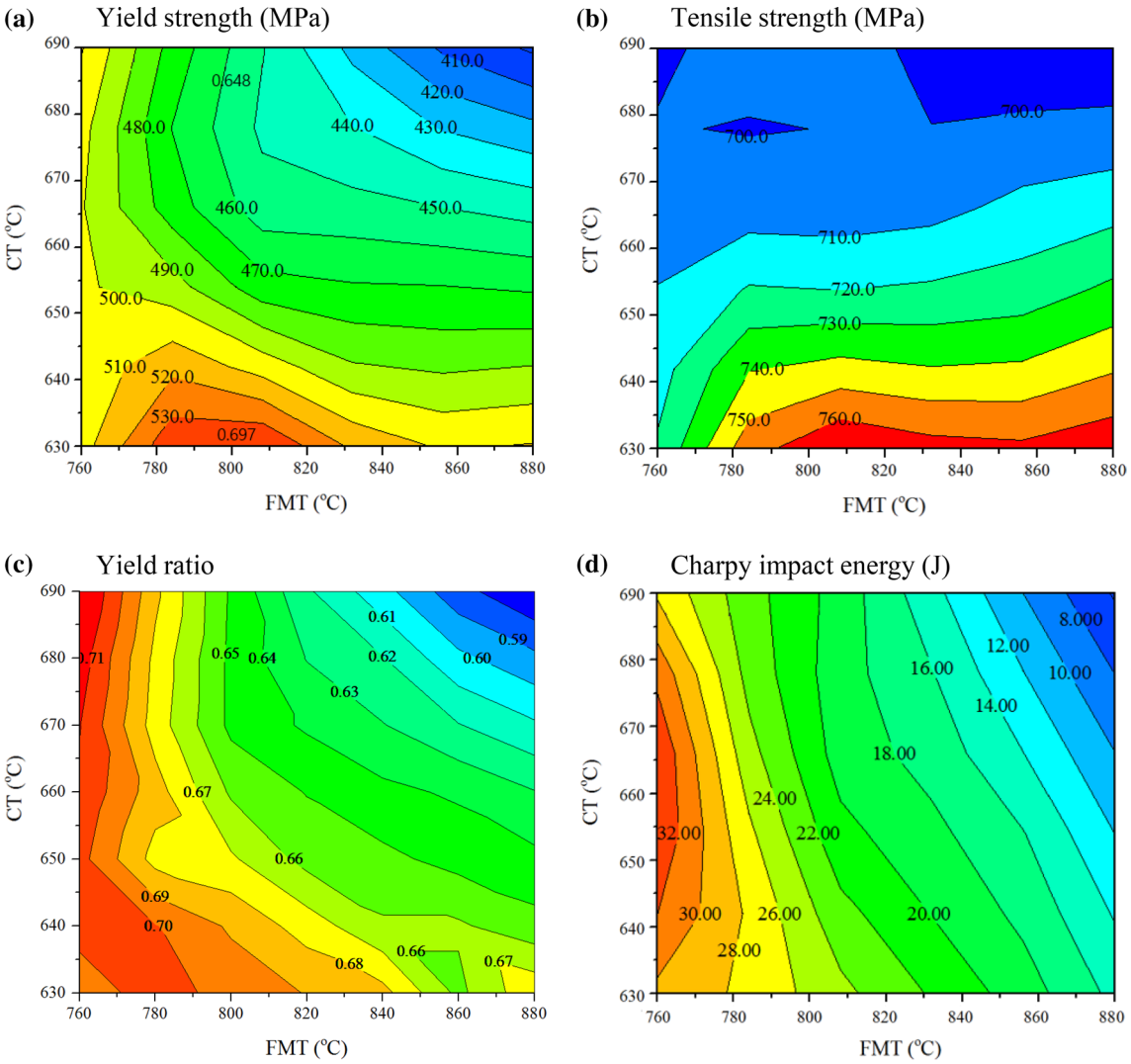

Fig. 1 Variations in the mechanical properties (**a** yield strength, **b** tensile strength, **c** yield ratio, and **d** Charpy impact energy value) of the steel plates with the finishing mill and coiling temperatures (FMT and CT, respectively)

map (Fig. 1d) revealed a decreasing tendency as the FMT increased: moreover, the impact energy was very low (less than 10 J) when both the CT and the FMT were high.

Figure 2 shows optical micrographs of these plates. At a given CT, both grain size and volume fraction of pearlite increased with increasing FMT. By contrast, when the FMT

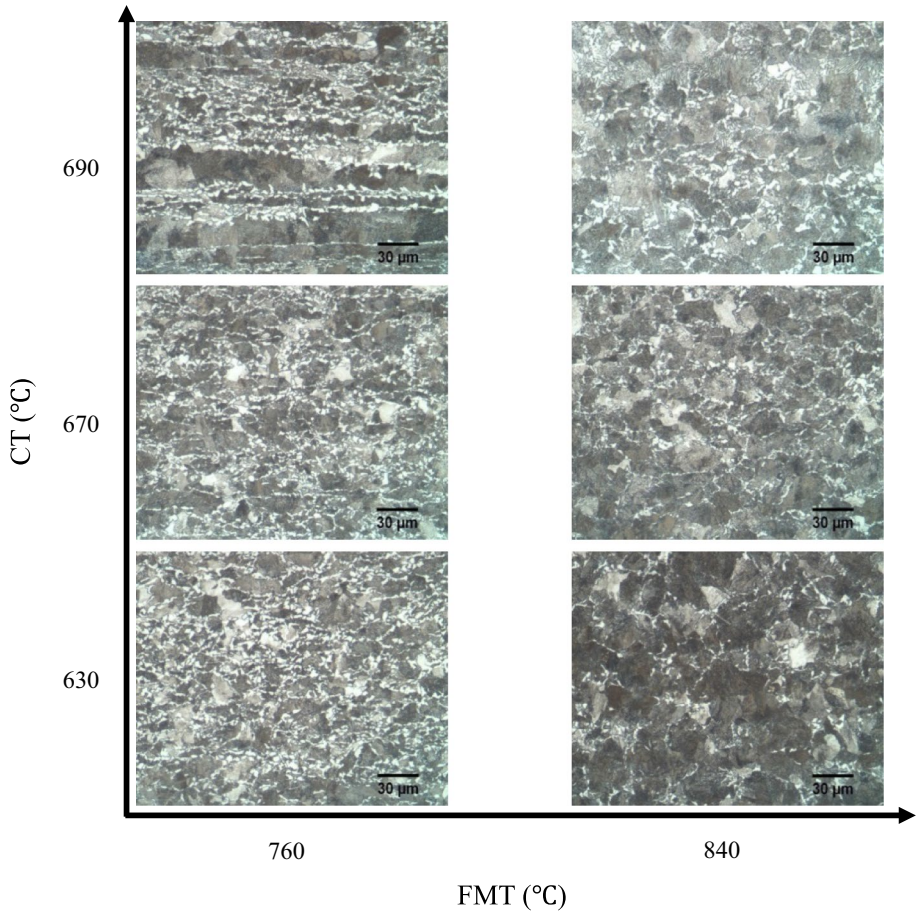

Fig. 2 Optical micrographs showing the microstructure of the steel plates fabricated under different finishing mill and coiling temperatures (FMT and CT, respectively)

was 840 °C, the grain size and volume fraction of pearlite decreased with increasing CT. The plates fabricated at an FMT of 760 °C contained a substantial amount of the ferrite phase irrespective of the CT because the rolling process was carried out below the austenitic temperature (Ar3). These results indicate that the size and amount of ferrite and pearlite phases are strongly dependent on the CT and FMT conditions. Therefore, the tensile and impact properties might have been strongly influenced by these differences in microstructure induced by the variation of the FMT and the CT. Details regarding the microstructure are discussed later in this section.

The medium-carbon steel used for the strain-based design must have a low YR, in accordance with its intended application; in addition, it should possess a sufficient impact toughness (greater than 10 J) to be used as structural pipes [21]. Therefore, in the present study, the optimal manufacturing conditions based on the mechanical properties of the plates produced under each condition were examined to determine whether they meet the properties required for the final products. First, the plates had to be produced at an FMT greater than 780 °C to obtain a low YR (Fig. 1c); however, an excessively high FMT should be avoided to ensure an impact toughness of 10 J or more (Fig. 1d). In addition, the CT should be set so that the YR and impact toughness are approximately 0.67 and greater than 15 J, respectively. On the basis of these considerations, two FMT/CT combinations were chosen: (1) FMT of 800 °C and CT of 690 °C (denoted as FMT800-CT690) and (2) FMT of 880 °C and CT of 630 °C (denoted as FMT880-CT630). The mechanical properties of both the hot-rolled strips produced under these conditions and the pipes fabricated using these same strips will be discussed later, along with their relationship with the manufacturing conditions.

Figure 3 shows optical micrographs of the FMT800-CT690 and FMT880-CT630 strips. The ferrite volume fraction was higher in the FMT800-CT690 strip than in the FMT880-CT630 one because of the higher CT used for the former, which is consistent with its previously observed increase under conditions of increasing CT (Fig. 2). This CT dependence of the ferrite volume fraction can be explained on the basis of the continuous cooling transformation curve of the 0.4C–0.2Si–1.6Mn–0.1Cr (wt%) steel, which was obtained through dilatometric tests (Fig. 4): the ferrite phase began to form at ~640 °C, whereas the pearlite phase was mainly formed below 630 °C. Therefore, a substantial amount of ferrite was formed when the CT was 690 °C because its temperature passed through its transformation

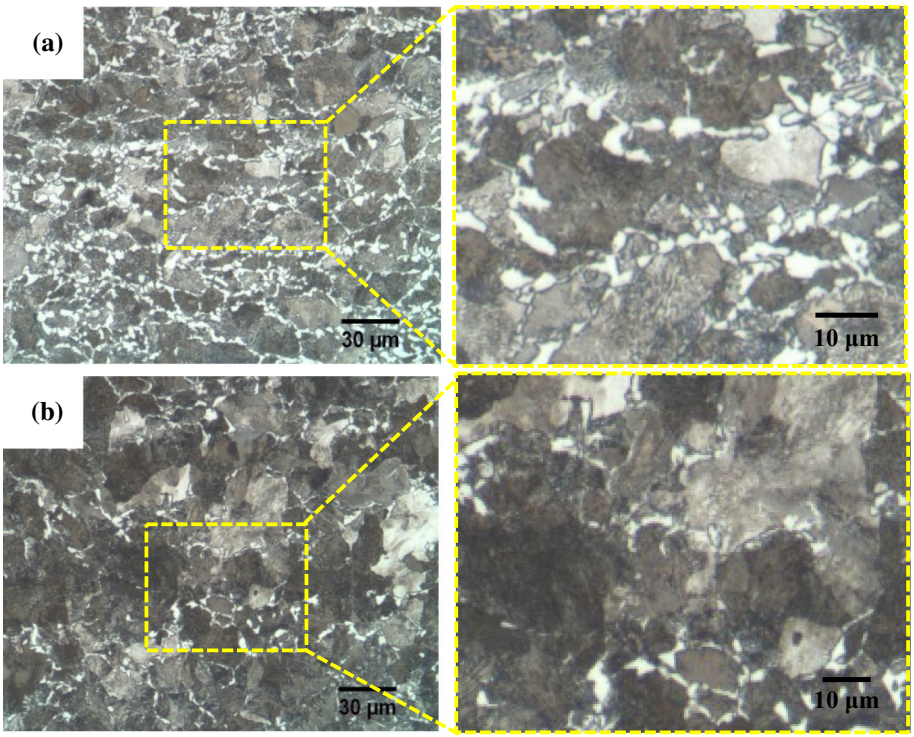

Fig. 3 Optical micrographs showing the microstructure of the steel strips fabricated under the two optimized combinations of finishing mill and coiling temperatures (FMT and CT, respectively): **a** FMT = 800 °C and CT = 690 °C and **b** FMT = 880 °C and CT = 630 °C

temperature region during the slow cooling process. However, when the coiling process was carried out at 630 °C, which is lower than the ferrite phase transformation temperature (640 °C), the resulting microstructure consisted mostly of the pearlite phase, in agreement with the results in Fig. 3b [22, 23]. Therefore, to form the amount of ferrite required to ensure good impact toughness, the coiling process should be conducted at a temperature above 650 °C if the phase transformation induced by deformation is not considered.

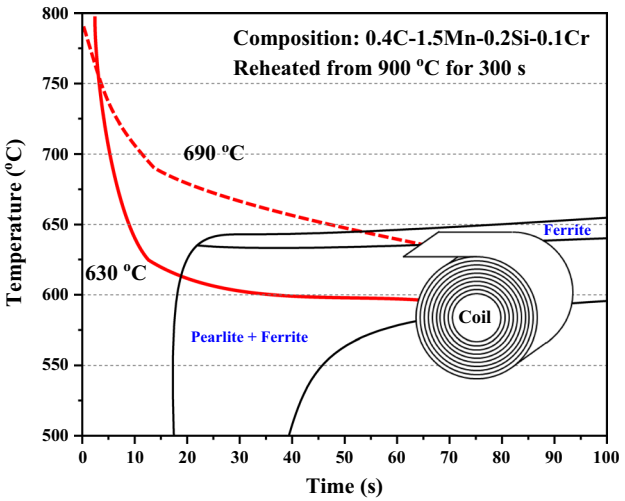

Fig. 4 Continuous cooling transformation curve of the 0.4C–0.2Si–1.6Mn–0.1Cr wt% steel

In the case of the FMT, its increase coarsened the grain size of the pearlite phase in the strips (Fig. 2). The grain size of the austenite phase formed in a high-temperature process affects the grain size of the pearlite phase because pearlite forms via phase transformation of the austenite phase during the finishing mill (FM) process. The lessening of the internal strain energy by austenite recrystallization and growth behaviors at high temperatures reduces the overall number of nucleation sites for the pearlite phase transformation, eventually degrading the mechanical properties of the hot-rolled steel product by forming coarse pearlite grains [24–27]. Therefore, the FM process should be conducted below the austenite recrystallization temperature to ensure a fine-grained microstructure; moreover, to restrict the abnormal grain growth induced by the nonuniform strain distribution that would result from two phases with different mechanical properties, the FM process should not be carried out in the austenite/ferrite two-phase region [28–30]. The FM process should accordingly be conducted at temperatures within the austenite single-phase region (i.e., above Ar3). The FM processes performed in the present study were started below 1000 °C and were completed at 880 or 800 °C. For the steel used in the present study, the nonrecrystallization temperature was calculated on the basis of the empirical equation suggested by Boratto et al. [31] by considering the C, Mn, Si, and Al contents. In addition, the Ar3 temperature for the two-phase region was derived on the basis of the alloying elements using the equation reported by Trzaska and Dobrazanski [32]; the Ar3 temperatures were greater

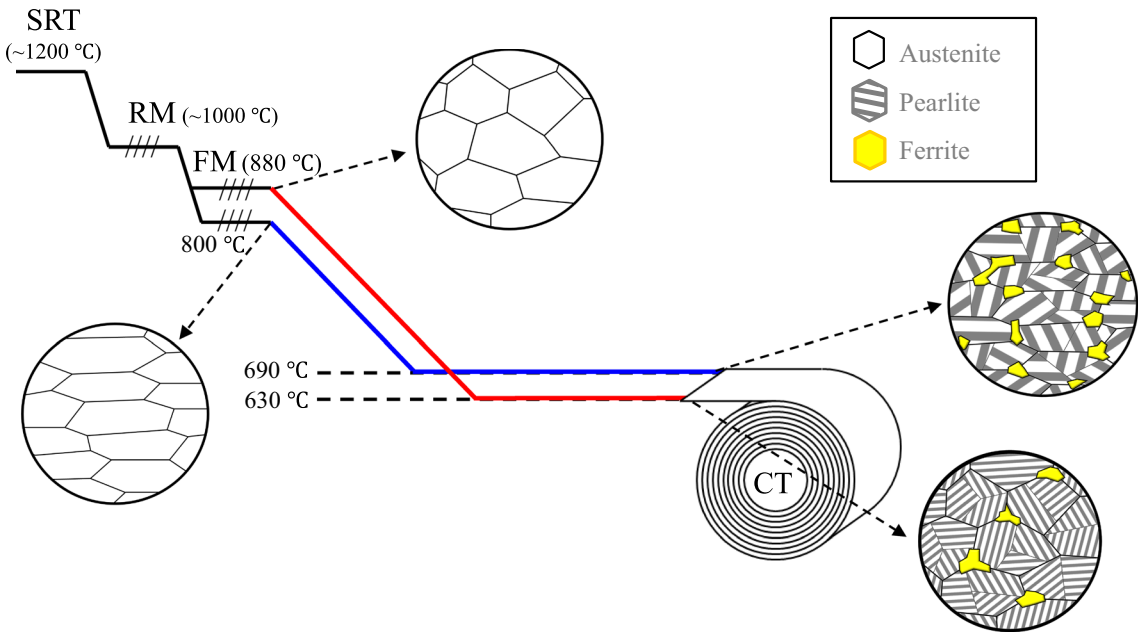

Fig. 5 Schematic of the microstructure evolution during the rolling process under different manufacturing conditions

than 1000 and ~780 °C, respectively. These results confirm that the FM process of the selected two conditions (i.e., FMT800-CT690 and FMT880-CT630) was carried out at temperatures (880 or 800 °C) suitable to suppress the recrystallization and complete the process above A3. In these cases, the microstructure consisted of only austenite phase during the entire FM process and the shape of the unrecrystallized austenite grains was gradually flattened through this process. The strained and elongated austenite grain structure has a large number of nucleation sites for the ferrite or pearlite phase transformation because of an increase in the grain-boundary fraction. The austenite grains showed a more flattened shape at FMT = 800 °C than at FMT = 880 °C because of the rolling process carried out at a lower temperature. This result means that the hot-rolled FMT800-CT690 strip had finer grains and a larger ferrite volume fraction than the FMT880-CT630 strip because of the increase of ferrite and pearlite nucleation sites induced by the more flattened austenite grains under the former condition (Fig. 3a and b). Moreover, the less flattened austenite grains observed at FMT = 880 °C coarsely evolved into pearlite transformation induced by the considerably lower CT (630 °C). That is, in the case of the FMT800-CT690, the austenite grains with a more flattened pancake-like shape were transformed into finer pearlite and ferrite grains compared with the FMT880-CT630 case. The aforementioned microstructure evolution with the manufacturing conditions are schematized in Fig. 5. In addition, the FMT800-CT690 strip exhibited a considerably higher impact toughness (46 J) than the FMT880-CT630 strip (28 J), which is mainly attributed to the grain refinement by the lower FMT of the FMT800-CT690 strip.

The tensile properties of the hot-rolled strips realized under these optimized conditions (FMT880-CT630 and FMT800-CT690), which exhibited a low YR and excellent impact toughness, and of the pipes fabricated using these strips are summarized in Table 3. The compressive strain (ε) applied to the hot-rolled strips during the pipe manufacturing process was derived from the relationship between the

Table 3 Mechanical properties of steel strips manufactured under two different manufacturing conditions (*FMT* finishing mill temperature, *CT* coiling temperature) and the pipes fabricated using these strips

Condition	Type of specimen	YS (MPa)	TS (MPa)	EL (%)	CVN (J)
FMT880-CT630	Strip	505	761	28.0	28
	508 mm pipe	555	733	27.2	–
	244 mm pipe	667	745	27.0	–
FMT800-CT690	Strip	454	755	27.5	46
	508 mm pipe	458	731	27.0	–
	244 mm pipe	545	725	26.3	–
Standard value		379–552	> 655	> 16	@ 0 °C

pipe diameter (D) and thickness (t) (i.e., $\varepsilon = t/D$); it was 4.1% and 2.0% for the 244 and 508 mm-diameter pipes, respectively. In the 508 mm-diameter pipe manufactured using the FMT880-CT630 strip, the yield strength increased by 50 MPa (from 505 MPa for the strip to 555 MPa for the pipe) because of the plastic deformation (2.0%) induced by the pipe manufacturing process. For the pipe with a smaller diameter (244 mm), the yield strength greatly increased to 667 MPa because of the increased compressive strain (4.1%); this result indicates that the strip, which was a nearly full pearlite phase, showed a sudden increase in yield strength when subjected to plastic deformation during the pipe manufacturing process. However, when the FMT800-CT690 strip was used, the yield strength of the 508 and 244 mm-diameter pipes was 458 and 545 MPa, respectively; in particular, the yield strength of the 508 mm-diameter pipe was nearly identical to that of the strip (454 MPa) (Table 3). This result indicates that the yield strength of the strip, which contained a substantial amount of ferrite phase, hardly increased when a compressive strain of 2.0% was applied. However, when the applied compressive strain was 4.1%, the yield strength considerably increased from 454 to 545 MPa because of work hardening.

For discussion of the difference in the yield strength increase as a function of the deformation strain, we present the tensile stress–strain curves of the FMT800-CT690 and FMT880-CT630 strips in Fig. 6, along with the reference yield strength range required for a low YR on the basis of the strain-based design concept. First, although the FMT880-CT630 strip exhibited a larger grain size than the FMT800-CT690 strip, its yield strength was greater because of its thinner s_c and its larger pearlite volume fraction due

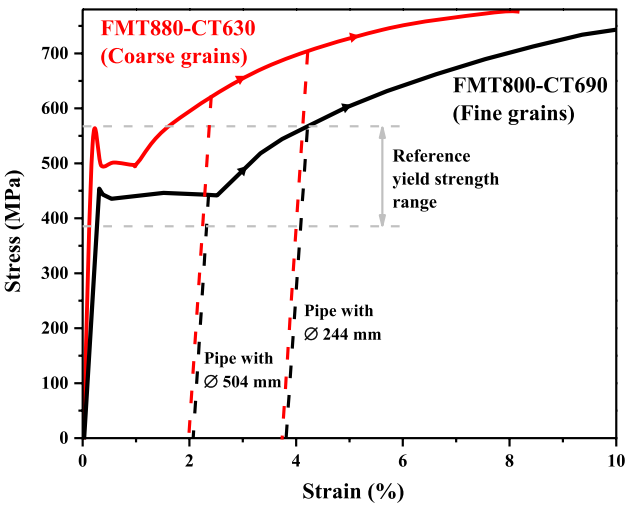

Fig. 6 Tensile stress–strain curves of the strips fabricated under two different combinations of finishing mill and coiling temperatures (FMT and CT, respectively): FMT = 800 °C and CT = 690 °C (black line) and FMT = 880 °C and CT = 630 °C (red line)

to its lower CT. The lamellar cementite layer in the pearlite phase acts as a barrier against dislocation movements and restricts the slip distance in the ferrite; accordingly, the yield strength in pearlite steel is especially determined by interlamellar spacing [33]. In addition, in ferrite–pearlite dual-phase steels, the yield strength increases with increasing volume fraction of pearlite phase [34]. Therefore, the FMT880-CT630 strip with the more abundant and narrower pearlite grains exhibits higher strength. Second, the yield-point phenomenon occurred during the tensile deformation in both strips. This phenomenon is related to the interaction between dislocations and interstitial solute atoms, such as carbon and nitrogen, and generally occurs in low-carbon steels containing phases with relatively low dislocation density, such as ferrite and pearlite. Because the steel strips used in the present study consisted precisely of ferrite and pearlite phases, they exhibited an obvious yield-point phenomenon. However, the yield-point elongation of the FMT800-CT690 strip was substantially larger than that of the FMT880-CT630 one.

As the grain size of ferrite decreases, the density of mobile dislocations formed during tensile deformation is decreased by the reduction in area of the dislocation source (i.e., the internal area of grains) and the recovery process during tension is promoted by the increased grain boundaries, which consequently leads to an increase in the yield-point elongation [35]. Accordingly, the greater yield-point elongation of the FMT800-CT690 strip is attributed to the combined effects of a finer grain structure, higher volume fraction of ferrite, and a wider lamellar spacing in the pearlite phase [35–38].

In relation to the aforementioned lamellar spacing, Fig. 7 shows that the associated microstructure depended on the CT when the FMT was fixed at 840 °C: specifically, the specimen processed at a CT of 690 °C exhibited a wider interlamellar spacing than that processed at 630 °C. According to numerous previous studies on s_c and the manufacturing conditions, the s_c value for the Fe–C system can be approximated as follows [39, 40]:

$$s_c = \frac{2\sigma^{\frac{\alpha}{\theta}} T^{eq}}{\Delta H_v \Delta T} \approx 6.13 \times 10^{-9} \frac{T^{eq}}{\Delta T}$$
$$\left(\sigma^{\frac{\alpha}{\theta}} = 0.93\ \mathrm{J/m^2}, \quad \Delta H_v = 607\ \mathrm{MJ/m^3}\right)$$

where $\sigma^{\alpha/\theta}$, T^{eq}, ΔT, and ΔH_v are the energy per unit area of the ferrite/cementite interface, the eutectoid temperature, the undercooling, and the enthalpy change, respectively. In addition, the phase transformation behavior of pearlite is conventionally expressed through the Kolmogorov–Johnson–Mehl–Avrami equation [41–45]:

$$X = X^e(1 - \exp(-k(t - \tau)^n)$$

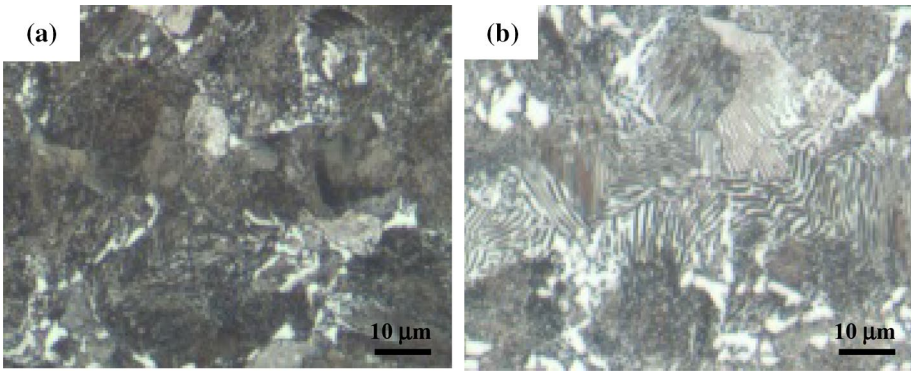

Fig. 7 Optical micrographs showing the lamellar spacing of the pearlite phase in the steel products fabricated under two different combinations of finishing mill and coiling temperatures (FMT and CT, respectively): **a** FMT = 840 °C and CT = 630 °C and **b** FMT = 840 °C and CT = 690 °C

where X is the fraction transformed, t is time, X^e and n are the thermodynamic equilibrium fraction and time exponent, both of which are fixed under the same transformation mechanism without considering the temperature range, respectively, and k and τ are respectively the rate constant and the incubation time, both of which are generally related to microstructure, chemical composition, and temperature. To calculate the interlamellar spacing and volume fraction of the pearlite phase in the steel used in this study, the required values for the two abovementioned equations were obtained using the Thermo-Calc software and the data reported by Kwon et al. [46]. The calculation results are shown in Fig. 8 and correspond to the experimental results presented in Figs. 2 and 7. Because s_c is inversely proportional to the degree of undercooling, it decreased with decreasing CT. Moreover, when the CT was high, a substantial amount of ferrite formed, along with pearlite with a large lamellar spacing. The impact toughness of steels increases with a reduction in the grain size and an increase in the pearlite lamellar spacing and ferrite volume fraction [47, 48]; therefore, the

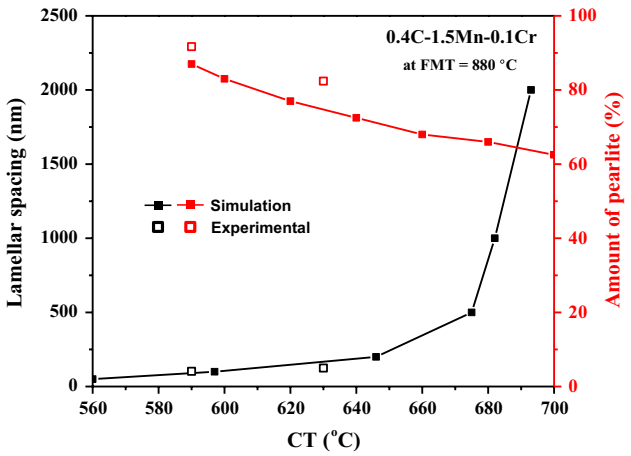

Fig. 8 Simulation results of the variations in lamellar spacing and in the amount of pearlite phase with the coiling temperature (CT), and experimental results obtained at CTs of 590 and 630 °C at a finishing mill temperature (FMT) of 880 °C

strips manufactured at higher CT exhibited superior impact toughness compared with the strips manufactured at lower CT because of the increased amount of the ferrite phase and the wider lamellar spacing. Furthermore, the yield-point phenomenon became more pronounced with increasing ferrite volume fraction. That is, the FMT800-CT690 specimen exhibited a greater yield-point elongation and a higher impact energy than the FMT880-CT630 specimen; however, the work-hardening exponents of the FMT800-CT690 and FMT880-CT630 specimens after yield deformation were similar because the main phase in both strips was the same (pearlite) despite their difference in lamellar spacing [49]. These results demonstrate that the manufacturing temperatures strongly affect the mechanical properties of the strips and final pipes.

Thus, given the strain applied to a strip during the pipe manufacturing process, the strip production at an FMT greater than 850 °C and a CT less than 650 °C is advantageous because it improves the productivity and results in superb toughness when the applied strain is less than 2%. However, under an imposed strain of 4%, the strips must be produced at a low FMT and a high CT to ensure a low YR and high impact properties through the formation of a wide lamellar spacing, fine grains, and a sufficient amount of ferrite.

4 Conclusions

This study has examined the dependence of the mechanical properties and microstructure of medium-carbon steel OCTG products on their rolling and coiling temperatures, leading to the following conclusions.

1. The YR, which is important for high workability, decreased with increasing FMT and CT, whereas the impact energy tended to decrease with increasing FMT. Therefore, two manufacturing conditions—specifically, FMT800-CT690 and FMT880-CT630—that provided

excellent mechanical properties were selected to confirm the good mechanical properties after the pipe manufacturing process.

2. The selected FMT and CT conditions were considered suitable on the basis of the austenite recrystallization and Ar3 temperatures. The FMT800-CT690 strip exhibited a finer grain structure and a higher ferrite volume fraction compared with the FMT880-CT630 strip because of the passing of the ferrite transformation region by high CT and the formation of flattened austenite grains by low FMT.
3. The FMT800-CT690 strip shows a lower yield strength and delayed work-hardening behavior compared with the FMT880-CT630 strip. In addition, the higher yield-point elongation of the FMT800-CT690 strip was attributed to its larger ferrite volume fraction, finer grain size, and wider lamellar spacing compared with those of the FMT880-CT630 strip. The FMT800-CT690 strip could satisfy the required yield strength specification even after substantial deformation of 4%.
4. The pearlite lamellar spacing was calculated from the relationship among interface energy, temperature, and enthalpy of the Fe–C system. The Avrami equation was used to predict the pearlite volume fraction from the conventional phase transformation behavior. The obtained values well matched the experimental results of increased lamellar spacing and decreased volume fraction with increasing CT.

Acknowledgements This work was supported by National Research Foundation of Korea (NRF) Grants funded by the Korean government (MSIP, South Korea) (Nos. 2017R1A4A1015628 and 2019R1A2C1085272).

References

1. Oil Country Tubular Goods (OCTG) Market in North America - Forecast, 2012-2019 (Micro-Market Moniter, 2014), http://www.micromarketmonitor.com/market/north-america-oil-country-tubular-goods-octg-9739477780.html
2. M. Katsumi, N. Yutaka, J.F.E. Tech, Rep. **7**, 1 (2006)
3. H. Brauer, H. Löbbe, in *Oil and Gas Pipelines*, ed. By R.W. Revie (John Wiley & Sons, New Jersey, 2015), p. 203
4. N. Y. Ghodsi, in *Oil and Gas Pipelines*, ed. By R.W. Revie (John Wiley & Sons, New Jersey, 2015), p. 37
5. M. Mitsuya, S. Sakanoue and H. Motohashi, in *Proceedings of the ASME 2012 Pressure Vessels and Piping Conference*, vol 8 (2012), p. 95
6. M. Hardy, Proc. Energy Mater. **2014**, 673 (2014)
7. Y. Hu, X. Zuo, R. Li, Z. Zhang, Mater. Res. **15**(2), 317 (2012)
8. C.C. Tasan, M. Diehl, D. Yan, M. Bechtold, F. Roters, L. Schemmann, C. Zheng, N. Peranio, D. Ponge, M. Koyama, K. Tsuzaki, D. Raabe, Ann. Rev. Mater. Res. **45**, 391 (2015)
9. X.S. Du, W.B. Cao, C.D. Wang, S.J. Li, J.Y. Zhao, Y.F. Sun, Mater. Sci. Eng. A **642**, 181 (2015)
10. M.A.M. Bonab, M. Eskandari, J.A. Szpunar, J. Mater. Res. **31**, 3390 (2016)
11. M.A.M. Bonab, H.G. Kucheki, Met. Mater. Int. **25**, 1109 (2019)
12. J. Zhou, D. Horsley, B. Rothwell, in *Proceedings of the International Pipeline Conference* (2006), p. 899
13. W. Mohr, in *Proceedings of the International Pipeline Conference* (2006), p. 899
14. S. Igi, T. Sakimoto, in *Proceedinsg of the 20th International Offshore and Polar Engineering Conference* (2010), p. 489
15. M. Lower, ORNL/TM-2014/106 of US DOE, p. 1 (2014)
16. A.J. Abdalla, L.R.O. Hein, M.S. Pereira, T.M. Hashimoto, Mater. Sci. Technol. **15**, 1167 (1999)
17. L. Himmel, K. Goodman, W.L. Haworth, *Fundamentals of Dual Phase Steels* (AIME, New York, 1981), p. 305
18. S. Gunduz, Mater. Sci. Eng. A **486**, 63 (2008)
19. R.G. Davies, R.A. Kot, B.L. Bramfitt, *Fundamentals of Dual Phase Steels* (AIME, New York, 1981), p. 265
20. S. Gunduz, A. Tosun, Mater. Des. **29**, 1914 (2008)
21. API specification 5CT 9th ed. (American Petroleum Institute, 2012), https://www.api.org/~/media/files/certification/monogram-apiqr/program-updates/5ct-9th-edition-purch-guidelines-r1-20120429.pdf
22. C.G. Andre, F.G. Caballero, C. Capdevila, L.F. Lvarez, Mater. Charact. **48**, 101 (2002)
23. K.B. Matus, G. Altamirano, A. Salinas, A. Flores, F. Goodwin, Metals **8**(9), 674 (2018)
24. Z. Cui, Ph.D. Thesis, The University of Sheffield (2016)
25. E.J. Palmiere, C.I. Garcia, A.J. Deardo, Metall. Mater. Trans. A **27**, 951 (1996)
26. S. Vervynckt, K. Verbeken, B. Lopez, J.J. Jonas, Int. Mater. Rev. **57**, 187 (2012)
27. L. Sun, Ph.D. Thesis, University of Sheffield (2012)
28. H. Tamotsu, S. Takeaki, O. Hiroo, Tetsu-to-Hagane **65**(9), 1425 (1979)
29. K. Maeda, T. Zhou, H.S. Zurob, Proc. TMS **2014**, 927 (2014)
30. K. Mukherjee, S.S. Hazra, M. Militzer, Metall. Mater. Trans. A **40**, 2145 (2009)
31. F. Boratto, R. Barbosa, S. Yue, J.J. Jonas, Proc. THERMEC **88**, 383 (1988)
32. J. Trzaska, L.A. Dobrazanski, J. Mater. Process. Technol. **192–193**, 504 (2007)
33. J.P. Houin, A. Simon, G. Beck, Trans. Iron Steel Inst. Jpn **21**(10), 726 (1981)
34. R. Mizuno, H. Matsuda, Y. Funakawa, Y. Tanaka, Tetsu-to-Hagané **96**(6), 414 (2010)
35. N. Tsuchida, T. Inoue, H. Nakano, T. Okamoto, Mater. Lett. **160**, 117 (2015)
36. T.L. Russell, D.S. Wood, D.S. Clark, Acta Metall. **9**, 1054 (1961)
37. R. Song, D. Pong, D. Raabe, J.G. Speer, D.K. Matlock, Mater. Sci. Eng. A **441**, 1 (2006)
38. R. Song, D. Ponge, D. Raabe, Scr. Mater. **52**(11), 1075 (2005)
39. J.J. Kramer, G.M. Pound, R.F. Mehl, Acta Metall. **48**(6), 763 (1958)
40. A.S. Pandit, Ph.D. Thesis, University of Cambridge (2011)
41. M. Avrami, J. Chem. Phys. **7**, 1103 (1939)
42. M. Avrami, J. Chem. Phys. **8**, 212 (1940)
43. M. Avrami, J. Chem. Phys. **9**, 177 (1941)
44. A.N. Kolmogorov, Izv Acad Nauk SSSR. Ser Mat. **3**, 355 (1937)
45. W.A. Johnson, R.F. Mehl, Trans. AIME **135**, 416 (1939)
46. O. Kwon, K.J. Lee, K.B. Kang, J.K. Lee, P.J. Lee, Y.S. Park, E.K. Ro, K.J. Min, J.D. Lee, K.C. Yoo, J. Korean Inst. Met. Mater. **30**(11), 1335 (1992)
47. J.M. Hyzak, I.M. Bernstein, Metall. Trans. A **7**(8), 1217 (1976)
48. T. Gladman, I. Mclvor, F. Pickering, J. Iron Steel Inst. **210**, 916 (1972)
49. V.I. Izotov, V.A. Pozdnyakov, E.V. Lukyanenko, O.Y. Usanova, G.A. Filippov, Phys. Met. Metallogr. **103**, 519 (2007)